

Research Article

Transmissivity Identification by Combination of CVFEM and Genetic Algorithm: Application to the Coastal Aquifer

Hassan Smaoui ^{1,2}, Abdelkabir Maqsoud,³ and Sami Kaidi^{1,2}

¹CEREMA/DTecEMF, 134, Rue de Beauvais, CS 60039, 60280 Margny-Lès-Compiègne, France

²Sorbonne Université, Université de Technologie de Compiègne, Laboratoire Roberval/LHN, FRE-CNRS 2012, CS 60319, 60203 Compiègne, France

³Université du Québec en Abitibi-Témiscamingue (UQAT) 675, 1^{ère} Avenue, Val-d'Or (QC) J9P 1Y3, Canada

Correspondence should be addressed to Hassan Smaoui; hassan.smaoui@cerema.fr

Received 31 December 2018; Accepted 11 June 2019; Published 29 July 2019

Academic Editor: Saeed Eftekhari Azam

Copyright © 2019 Hassan Smaoui et al. This is an open access article distributed under the Creative Commons Attribution License, which permits unrestricted use, distribution, and reproduction in any medium, provided the original work is properly cited.

The solution of inverse problems in groundwater flow has been massively invested by several researchers around the world. This type of problem has been formulated by a constrained optimization problem and this constraint is none other than the direct problem (DP) itself. Thus, solving algorithms are developed that simultaneously solve the direct problem (Darcy's equation) and the associated optimization problem. Several papers have been published in the literature using optimization methods based on computation of the objective function gradients. This type of method suffers from the inability to provide a global optimum. Similarly, they also have the disadvantage of not being applicable to objective functions of discontinuous derivatives. This paper is proposed to avoid these disadvantages. Indeed, for the optimization phase, we use random search-based methods that do not use derivative computations, but based on a search step followed only by evaluation of the objective function as many times as necessary to the convergence towards the global optimum. Among the different algorithms of this type of methods, we adopted the genetic algorithm (GA). On the other hand, the numerical solution of the direct problem is accomplished by the CVFEM discretization method (Control Volume Finite Element Method) which ensures the mass conservation in a natural way by its mathematical formulation. The resulting computation code HySubF-CVFEM (Hydrodynamic of Subsurface Flow by Control Volume Finite Element Method) solves the Darcy equation in a heterogeneous porous medium. Thus, this paper describes the description of the integrated optimization algorithm called HySubF-CVFEM/GA that has been successfully implemented and validated successfully compared to a schematic flow case offering analytical solutions. The results of this comparison are qualified of excellent accuracy. To identify the transmissivity field of the realistic study area, the code HySubF-CVFEM/GA was applied to the coastal "Chaouia" groundwater located in Western of Morocco. This aquifer of high heterogeneity is essential for water resources for the Casablanca region. Results analysis of this study has shown that the developed code is capable of providing high accuracy transmissivity fields, thus representing the heterogeneity observed *in situ*. However, in comparison with gradient method optimization the HySubF-CVFEM/GA code converges too slowly to the optimal solution (large CPU-time consuming). Despite this disadvantage, and given the high accuracy of the obtained results, the HySubF-CVFEM/GA code can be recommended to solve in an efficient and effective manner the identification parameters problems in hydrogeology.

1. Introduction

The coastal aquifers play an important role in the socio-economic development of the coastal plains [1–4]. These coastal aquifers are particularly exposed to over-exploitation problems that can induce aquifer salinization [5–7]. Also, as presented in the Intergovernmental Panel on climate change (IPCC, 2007), climate changes will provide variations in the

sea level, temperature and rate and intensity of precipitation. All these changes will affect freshwater resources, in terms of both quantity and quality [8].

The climate change impacts are mainly evaluated using numerical groundwater modeling for both flow and transport phenomenon (Moustadraf et al., 2008). The numerical groundwater modeling requires many hydrodynamic parameters such as the water budget, the storativity, the

piezometric level (also called the head), the transmissivity, and specific yield. These parameters are usually obtained from some in situ pumping field and/or laboratory tests. However, in situ measurements, which are usually performed in a limited number of points of the study area (due to their cost), may prove insufficient to deduct the transmissivity coefficient. Besides this major inconvenience we also note the difficulty of the logistic realization of the measurement itself (access to the measurement site). Consequently, measurements can be considered as not economically feasible especially in the case where the funds for scientific research are very limited.

Given these drawbacks, mathematical models have emerged as powerful tools to complete lack of information to estimate correctly the transmissivity coefficient. With the spectacular advances in information technology, the mathematical models combined with the optimization tools became essential for geosciences modeling including flows and associated transport in groundwater.

To ensure an optimal management of the groundwaters, we need a good estimation of the head obtained by solving the Darcy's equation. The quality of this estimation depends strongly on the quality of the transmissivity values (main flow parameter). However, the accurate knowledge of this parameter is difficult to obtain because of the heterogeneity due to real geological formation of the aquifers and the nature of the flows, or both. Consequently, the mathematical models and their discretization methods must be chosen judiciously in order to best approximate the studied phenomena. For a known transmissivity field, several codes solving Darcy's equation have been proposed to compute the hydraulic potential (see for example PMWIN-MODFLOW, FEFLOW, GMS, HySuf-FEM). This is called "the direct problem". However, a good prediction of the head requires prior identification of parameters involved in the Darcy's equation (this is "the inverse problem").

For over four decades inverse problem for groundwater flow has been studied by different authors (here, we cite only more recent studies: Katsifarakis et al., 1999; [9–16]) and a good review of this strategy to solve the problem can be seen in Yeh, 1986 and Carerra, 1988 [17, 18]. The strategy to identify the parameters by inverse problem consists of a combination of a computer code for flow (hydrodynamic model) and an optimization computer code. The optimization procedure was approached by a large number of optimizers: deterministic ones as gradient-based methods, Newton methods, quasi-Newton with interior points methods or stochastic ones as evolution strategies (ESs), artificial neural network (ANN) or genetic algorithms (GAs). The flow can be performed by different approximation methods as finite difference method (FDM), finite element method (FEM), finite volume method (FVM), meshless method, and many others.

In this paper, the CVFEM was chosen to compute the hydraulic head. This choice was motivated by the ability of this method to conserve the physical quantities involved in the hydrodynamic model (as FVM) and also by its ability to handle complex boundaries of the study area (as FEM). For the optimization step, we adopted the genetic algorithm. Although this type of algorithm is slower compared to

other algorithms (gradient-based algorithms), GA has been selected in this paper for its capacity to converge to a global optimum without using derivatives of the objective, also because it is well suited in particular on non-convex, non-separable, ill-conditioned, multi-modal or noisy objective functions. In addition, note that the inverse problem in groundwater flow is characterized by the identification of the large-size parameters (number of mesh node of the direct problem). It is also characterized by an objective function having no analytical expression, but built from the simulation results from the hydrodynamic model. These characteristics make usually the inverse problem in groundwater flow impossible to resolve by conventional deterministic methods. This is another reason which motivated our choice on a stochastic method particularly the GA.

This paper is organized as follows: Section 2 outlines the mathematical formulation that describes the CVFEM method for the direct problem and the GA for optimization procedure. Section 3 is devoted to the presentation of numerical results (academic tests) on the validation of the direct problem and the coupling "direct problem/optimization" procedure. At the end of this section we present the application of the combination "CVFEM/GA" to the realistic case of a coastal aquifer to determine the transmissivity field. Finally, discussion and conclusions are presented in the last section.

2. Mathematical Model

At the macroscopic scale, the rate at which the water flow in a soil is quantified using a variable that is referred to as the Darcy velocity or specific discharge \vec{q} . This variable, which has the dimensions of velocity, is defined as the discharge per unit cross area of soil that includes both the pore space and the grains in a flow section. It is also defined as a vector in the direction of flow, where its magnitude is equal to the volume of water flowing per unit time through a unit cross-sectional area normal to the direction of flow.

2.1. Governing Equations. Assume that the flow is stationary or that both fluid and porous media are incompressible. By the mass conservation law, the continuity equation holds, i.e.,

$$\nabla \cdot \vec{q} = f \quad (1)$$

where the function f represents sources or/and sinks terms.

Inside the saturated zone if we assume that the specific discharge \vec{q} is derived from a potential φ via the hydraulic conductivity tensor $\overline{\overline{K}}$, we obtain the unsteady Darcy law given by

$$\frac{\partial \varphi}{\partial t} - \nabla \cdot (\overline{\overline{K}} \nabla \varphi) = S \quad (2)$$

where S is the source (or sink) term.

An exact solution of a potential flow problem (2) can be derived only in special cases. Therefore, numerical methods are the major tool for solving such problems in practice. A

common approach is to rewrite this into the following partial differential equation (PDE) with its boundary conditions:

$$(\mathbf{DP}) \begin{cases} \frac{\partial \varphi}{\partial t} - \nabla \cdot (\overline{\mathbf{K}} \nabla \varphi) = S & \text{in } \Omega \\ \varphi = \varphi_D & \text{in } \partial\Omega_D \\ \vec{n} \cdot \vec{q} = \varphi_N & \text{in } \partial\Omega_N \\ \varphi(x, 0) = \varphi_0(x) & \text{in } \Omega \end{cases} \quad (3)$$

where Ω is the domain area, $\partial\Omega_D$ is the boundary of the imposed Dirichlet condition, $\partial\Omega_N$ is the boundary of the imposed Neumann condition, and \vec{n} is the outward normal vector to the Neumann boundary $\partial\Omega_N$. The equation (3) is known by Darcy equation. The average velocity \vec{v} of the fluid can be deduced from \vec{q} by $\vec{v} = \vec{q}/p$, where p is the porosity of the studied area. Otherwise, we note that, according to Ciarlet, [21], the problem (3) is a well-posed problem; i.e., the solution exists, is unique, and depends continuously on the data.

The vast majority of solvers of the Darcy equation use finite difference, finite volume, or finite element approximation in space. Numerous numerical approaches can be enumerated for solving equation (3). All these approaches are based on a discrete partition of the spatial domain of interest. The partition can be a structured grid or more generally an unstructured mesh. The numerical scheme that approximates the solution then consists in proposing an approximation of this solution on the discretized domain. In other words, we constrain the approximate solution to verify the Darcy equation to achieve a linear system (or non-linear) whose approximate solution is the unknown of such a system. The Darcy equation has been massively solved by classical methods (MDF, MEF, MVF). It is difficult to conclude on the effectiveness of this or that method, but it all depends on what one wishes to privilege between mass conservation, accuracy or a minimum computation (CPU time) [22, 23]. Today, we are witnessing a great growth in the use of CFD to solve real problems (environmental, industrial, etc.). To take into account the irregular boundaries of this type of problem, it has become necessary to choose discretization methods allowing flexibility in the management of boundary conditions on boundaries of complex geometries. Some numerical methods based on orthogonal or curvilinear coordinate structured meshes approaching boundaries are frequently used to calculate flows in irregular geometries, with satisfactory results. However, we also observe that methods based on unstructured finite element meshes have become the reference methods for the prediction of flows in complex geometries.

In this work and to solve the Darcy equation, we adopt the CVFEM method on a FEM type unstructured mesh. In CFD, this method combines the advantages of finite volume methods over regular mesh and finite element methods. Indeed, the CVFEM formulation in terms of flows only translates the physical principle of the local and global conservation of a quantity evolving in a volume of elementary control. But in particular, CVFEM allows efficient handling of pressure/velocity coupling. On the other hand, when

CVFEM is formulated on a finite element mesh, we inherit the geometric flexibility and the use of the basis functions of the Sobolev space to interpolate the solution on a control volume [24, 25].

2.2. The CVFEM Discretization. Before beginning the mathematical formulation of this method, a brief description of some spaces is necessary. Consider a limited open set $\Omega \subset \mathbb{R}^2$ having an Lipschitzian and continue boundary $\partial\Omega$. We define $L^2(\Omega)$ as being the space of real functions u such u^2 is measurable functions. square. We define $H^1(\Omega)$ also as the subset containing functions of $L^2(\Omega)$ whose first derivatives are also in $L^2(\Omega)$. Similarly, we define $H_g^1(\Omega)$ the subset of $H^1(\Omega)$ whose functions are equal to g on the on the boundary $\partial\Omega$ of Ω . Finally, we define the inner product of the space of $L^2(\Omega)$

$$\forall u, v \in L^2(\Omega) \quad (4)$$

$$(u, v)_{L^2(\Omega)} = \int_{\Omega} u(x) v(x) dx$$

The numerical solution of equation (3) begins with the arbitrary subdivision of the domain Ω into N_e elements (for example triangular elements) denoted $(T_k)_{k=1, \dots, N_e}$ and N_n nodes. The family of triangles T_k forms what is called the triangulation \mathcal{T}_h , indexed by the parameter h which designates the length of the largest sides of all the triangles of the mesh. This triangulation admits N_n nodes which are the vertices of the set of triangles covering the domain. In the rest of this document, we omit the subscript “ k ” of the triangle T_k , but for any triangle we will note $T \in \mathcal{T}_h$. The triangulation \mathcal{T}_h allows the approximation of the domain Ω by $\Omega_h = \bigcup_{T \in \mathcal{T}_h} T$. We can now give the piecewise linear finite element spaces by

$$H_h = \{v \in \mathcal{C}^0(\Omega_h) : \forall T \in \mathcal{T}_h, v|_T \text{ is linear}\} \quad (5)$$

where $\mathcal{C}^0(\Omega_h)$ is the set of continuous functions on Ω_h and $v|_T$ is the restriction of the function v on the triangle T . In the same manner, we define $H_{h,g}(\Omega) = H_h \cap H_g^1(\Omega)$.

The CVFEM method must be applied to the integral formulation of the Darcy equation. This formulation translates the physical principle of the conservation of the φ transferred scalar quantity in the small control volume \mathcal{V} .

$$\int_{\mathcal{V}} \frac{\partial \varphi}{\partial t} dv - \int_{\mathcal{V}} \nabla \cdot (\overline{\mathbf{K}} \nabla \varphi) dv = \int_{\mathcal{V}} S dv \quad (6)$$

To preserve this important physical principle in the numerical results, CVFEM uses a weighting function equal to the unit on all the volume of control associated with the node of the computation and zero elsewhere. Consequently, the CVFEM discretization imposes naturally the physical principle of conservation in the control volume \mathcal{V} . Thus, the CVFEM admits an easy physical interpretation and its numerical solution meets the requirements of conservation both locally and globally even in the case of use of a coarse mesh.

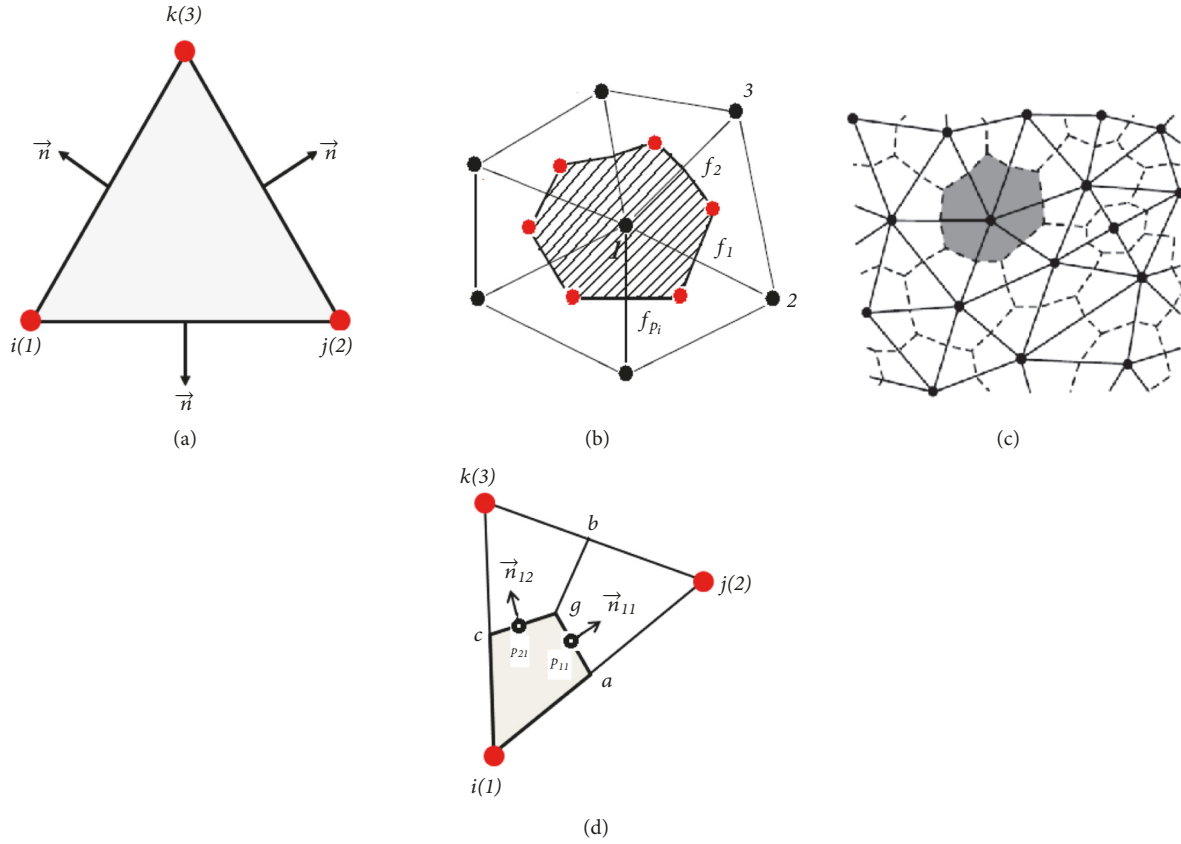


FIGURE 1: The construction of control volumes: (a) the cell-centered control volume; (b) the vertex-centered control volume, (c) the dual mesh and (d) the sub-control volume. Notation $(i(1), j(2), k(3))$ means that for a triangle T , the global numbering is (i, j, k) and the local numbering is $(1, 2, 3)$.

CVFEM uses two volume control types: cell-centered volume control and vertex-centered volume control. The first type is to consider the triangular element as a control volume (Figure 1(a)), while the second type builds support around a node i to use the dual mesh (Figure 1(c)). Several methods have been used for the construction of the control volume \mathcal{V}_i based on the support of nodes i . As far as we are concerned, we use volumes of controls of the dual mesh built as follows: for a node i of the mesh, one searches all the triangles having common node i . So the control volume \mathcal{V}_i will be formed by joining the centers of gravity of all the triangles around the node i (Figure 1(b)). It is considered that the boundary $\Gamma_i = \partial\mathcal{V}_i$ of the control volume \mathcal{V}_i consists of p_i elementary facets f_m . We note the set of these facets by \mathcal{F}_i ($\text{card}(\mathcal{F}_i) = p_i$). It should be noted that if the control volume \mathcal{V}_i is constructed from p_i triangles, then \mathcal{V}_i is the union of p_i sub-control volume $(\mathcal{S}_{i,m})_{m=1,p_i}$ which is the quadrilateral (iagc) (See Figure 1(d)).

2.3. The Control Volume Formulation. After the step of the studied area discretization in elementary control volume, the different numerical methods of approximations consist in approaching the solution on the mesh nodes based on the physical principle of conservation. Like the other methods CVFEM applies this principle on the control volume \mathcal{V}_i to

the equation (6). By using the Gauss divergence theorem, we have

$$\int_{\mathcal{V}_i} \frac{\partial \varphi}{\partial t} dv - \int_{\partial\mathcal{V}_i} (\overline{\mathbf{K}} \nabla \varphi) \cdot \vec{n} dl = \int_{\mathcal{V}_i} S dv \quad (7)$$

where \vec{n} is the outward unit normal vector to $\partial\mathcal{V}_i$. For a physical quantity ψ , the control volume average is defined by

$$\bar{\psi}_i = \frac{1}{\text{mes}(\mathcal{V}_i)} \int_{\mathcal{V}_i} \psi dv \quad (8)$$

where $\text{mes}(\mathcal{V}_i)$ is the volume of \mathcal{V}_i (in 2D computation $\text{mes}(\mathcal{V}_i) = \text{area}(\mathcal{V}_i)$). Since $\mathcal{V}_i = \bigcup_{m=1}^{p_i} \mathcal{S}_{i,m}$, the integral (7) can be written in its discrete form by

$$\bar{\psi} = \frac{1}{\text{mes}(\mathcal{V}_i)} \sum_{m=1}^{p_i} \hat{\psi}_m \delta_m \quad (9)$$

where δ_m is the volume of the sub-control volume $\mathcal{S}_{i,m}$ and $\hat{\psi}_m$ is the average value of ψ in $\mathcal{S}_{i,m}$. Note that, for the clarity of the notation, we omit the bar from the average values of

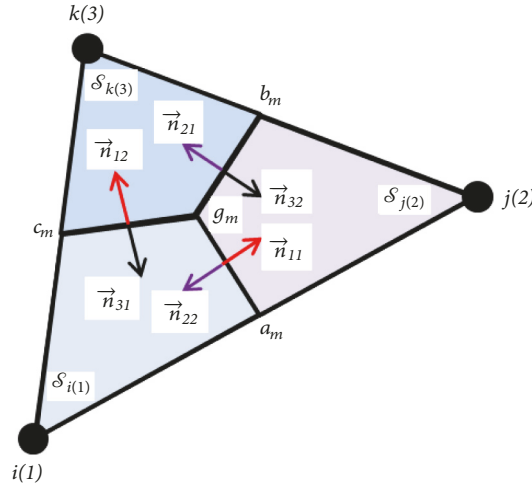


FIGURE 2: Three sub-control volumes $\mathcal{S}_{i(1)}$, $\mathcal{S}_{j(2)}$, $\mathcal{S}_{k(3)}$ contributing to the three control volume $\mathcal{V}_i, \mathcal{V}_j, \mathcal{V}_k$.

the variables. With these notations, equation (6) is written in discrete form:

$$\begin{aligned} \frac{\partial \varphi_i}{\partial t} \text{mes}(\mathcal{V}_i) - \sum_{m \in \mathcal{F}_i} \int_{f_m} [\overline{\mathbf{K} \nabla \varphi}]_{f_m} \vec{n}_m dl \\ = S_i \text{mes}(\mathcal{V}_i) \quad \forall i = 1, \dots, N_n \end{aligned} \quad (10)$$

Note that the approximation space $H_{h,g}(\Omega)$ is a vector space of finite dimension ($\dim(H_{h,g}(\Omega_h)) = N_n$). This space then admits piecewise affine basis functions noted as $(\psi_m)_{m=1, \dots, N_n}$. The construction of this basis functions is based on the Lagrange interpolation function given by

$$\begin{aligned} \forall i = 1, \dots, N_n, \\ \forall m = 1, \dots, N_n \\ (x_m, y_m) \in \Omega_h, \\ \psi_i(x_m, y_m) = \begin{cases} 1 & \text{if } i = m \\ 0 & \text{if } i \neq m \end{cases} \end{aligned} \quad (11)$$

Consequently, for $\varphi \in H_{h,g}(\Omega_h)$ and for $(x, y) \in T$, we can write $\varphi(x, y) = \sum_{m=1}^3 \varphi_m \psi_m(x, y)$. It is quite clear that the gradient $\nabla \varphi$ that appears in the integral term in equation (10) is constant ($\nabla \varphi(x, y) = \sum_{m=1}^3 \varphi_m \nabla \psi_m(x, y)$) since the basis functions $(\psi_m)_{m=1, \dots, N_n}$ are affine on each triangle of the mesh. By using one-point Gauss quadrature method, an approximation of equation (10) is

$$\begin{aligned} \frac{\partial \varphi_i}{\partial t} \text{mes}(\mathcal{V}_i) - \sum_{m \in \mathcal{F}_i} [\overline{\mathbf{K} \nabla \varphi}]_{f_m} \vec{n}_m A_m = S_i \text{mes}(\mathcal{V}_i) \\ \forall i = 1, \dots, N_n \end{aligned} \quad (12)$$

where A_m is the length of the face f_m .

Expression (12) is the discrete algebraic equation of the linear system with the unknown φ_i that determines the solution of the Darcy equation. If we note by Ψ the solution vector of components $(\varphi_m)_{m=1, \dots, N_n}$, equation (12) can be written in matrix form as

$$\mathbf{M} \frac{\partial \Psi}{\partial t} + \mathbf{K} \Psi = \mathbf{b} \quad (13)$$

where \mathbf{M} is the diagonal mass matrix ($M_{ii} = \text{mes}(\mathcal{V}_i)$, $i = 1, \dots, N_n$), \mathbf{K} is the stiffness matrix and \mathbf{b} is the second member vector containing the source/sink term and the values of the boundary conditions.

The global matrix \mathbf{K} of the linear system is a sparse matrix. It is then necessary to adopt an optimal storage to store only the non-zero matrix coefficients. We recall that from the equation (12) we can naively construct the matrix \mathbf{K} line by line without storing the null coefficients, but this way of doing things proved to be very consuming in CPU time (much more than the CPU time to solve the linear system itself). The second way is to assemble the global matrix \mathbf{K} from the elementary matrices calculated on each control volume \mathcal{V}_i . However, the assembly step is very laborious to implement since the size of the elementary matrices p_i is not constant (p_i is the number of triangle around the node i). To avoid these two computationally time expensive methods of assembling the global matrix, we have adopted the conventional assembly procedure inherent in FEM. Indeed, we will consider the control volume \mathcal{V}_i , but we will calculate the elementary matrix on an isolated triangle from this control volume \mathcal{V}_i (Figure 2). For a triangle of vertex $(i(1), j(2), k(3))$, our method consists of computing the simultaneous contribution of the sub-control volume $\mathcal{S}_{i(1)}, \mathcal{S}_{j(2)}, \mathcal{S}_{k(3)}$ of the control volume $\mathcal{V}_i, \mathcal{V}_j, \mathcal{V}_k$, then one applies the classical FEM procedure of assembly of elementary matrices \mathbf{K}_T calculated on a triangle T . Note that the global matrix \mathbf{K} obtained by our method is identical to those obtained by the two methods

described above. Indeed, the boundary of the control volume $\partial\mathcal{V}_i$ can be written in two different ways, namely,

$$\partial\mathcal{V}_i = \bigcup_{m=1}^{p_i} f_m \quad (14)$$

$$\text{and } \partial\mathcal{V}_i = \bigcup_{m=1}^{p_i} \partial\mathcal{S}_{i,m} = \bigcup_{m=1}^{p_i} [a_m, g_m] \cup [g_m, c_m]$$

This is the second way to express \mathcal{V}_i which allowed us to assemble by the triangles constituting the control volume \mathcal{V}_i

2.4. The Elementary Matrix $\mathbf{M}_T, \mathbf{K}_T, \mathbf{b}_T$. To evaluate the elementary matrices \mathbf{M}_T et \mathbf{K}_T we consider the local numbering (1, 2, 3). Similarly, we assume that the studied porous medium is isotropic (the hydraulic conductivity tensor $\overline{\overline{\mathbf{K}}}$ is diagonal) and finally the interpolation functions $(\psi_i)_{i=1,2,3}$ are affine on each triangle. It should be noted that ψ_i are easily determined from the equation (11). Thus, these assumptions can be formulated by

$$\overline{\overline{\mathbf{K}}} = \begin{bmatrix} K_x & 0 \\ 0 & K_y \end{bmatrix} \quad (15)$$

and $\forall (x, y) \in T$,

$$\psi_i(x, y) = \alpha_i^T x + \beta_i^T y + \gamma_i^T \quad \text{for } i = 1, 2, 3$$

For each triangle T , the mass matrix \mathbf{M}_T is easy to evaluate. It is a main diagonal matrix whose diagonal coefficients are none other than the area of each sub-control volume \mathcal{S}_i (Figure 2).

$$\forall T \in \mathcal{T}_h, \quad \mathbf{M}_T = \begin{bmatrix} \text{mes}(\mathcal{S}_1) & 0 & 0 \\ 0 & \text{mes}(\mathcal{S}_2) & 0 \\ 0 & 0 & \text{mes}(\mathcal{S}_3) \end{bmatrix} \quad (16)$$

with $\text{mes}(\mathcal{S}_1) = \text{mes}(\mathcal{S}_2) = \text{mes}(\mathcal{S}_3) = \text{area}(T)/3$.

To explicit the coefficients of the elementary stiffness matrix \mathbf{K}_T , we apply the Gauss divergence theorem to the diffusive term of the equation (6), but this time successively to the control sub-volumes $\mathcal{S}_1, \mathcal{S}_2, \mathcal{S}_3$.

For Sub-Control Volume \mathcal{S}_1

$$\begin{aligned} \int_{\mathcal{S}_1} \nabla \cdot (\overline{\overline{\mathbf{K}}} \nabla \varphi) dv &= \int_{\partial\mathcal{S}_1} (\overline{\overline{\mathbf{K}}} \nabla \varphi) \vec{n} dl \\ &= \int_{[a,g]} (\overline{\overline{\mathbf{K}}} \nabla \varphi) \vec{n} dl \\ &\quad + \int_{[g,c]} (\overline{\overline{\mathbf{K}}} \nabla \varphi) \vec{n} dl \end{aligned} \quad (17)$$

By using the expression of $\overline{\overline{\mathbf{K}}}$, and the interpolation functions ψ_j , we can write

$$\varphi(x, y) = \sum_{j=1}^3 \varphi_j \psi_j(x, y) \quad (18)$$

$$\text{and } \nabla \varphi(x, y) = \sum_{j=1}^3 \varphi_j \nabla \psi_j(x, y) = \begin{bmatrix} \alpha_j^T \\ \beta_j^T \end{bmatrix}$$

$$\overline{\overline{\mathbf{K}}} \nabla \varphi \cdot \vec{n} = \sum_{j=1}^3 \varphi_j \begin{bmatrix} K_x & 0 \\ 0 & K_y \end{bmatrix} \begin{bmatrix} \alpha_j^T \\ \beta_j^T \end{bmatrix} \cdot \vec{n} \quad (19)$$

$$= \sum_{j=1}^3 \varphi_j (K_x \alpha_j^T n_x + K_y \beta_j^T n_y)$$

By adopting notation of the Figure 1(d), the integral term can be approximated by

$$\begin{aligned} \int_{[a,g]} (\overline{\overline{\mathbf{K}}} \nabla \varphi) \vec{n} dl + \int_{[g,c]} (\overline{\overline{\mathbf{K}}} \nabla \varphi) \vec{n} dl &= \sum_{j=1}^3 \varphi_j \\ &\cdot \left[(K_x \alpha_j^T n_{11}^x + K_y \beta_j^T n_{11}^y)_{p11} \ell_{11} \right. \\ &\quad \left. + (K_x \alpha_j^T n_{12}^x + K_y \beta_j^T n_{12}^y)_{p12} \ell_{12} \right] \end{aligned} \quad (20)$$

where ℓ_{11} and ℓ_{12} are respectively the length of the $[a, g]$ and $[g, c]$ segments, $p11$ and $p12$ are respectively the position of the middle of the $[a, g]$ and $[g, c]$ segments and n_{11}^x, n_{11}^y are then x-component and y-component of the normal vector \vec{n}_{11} . Note that all these parameters can be computed easily from the mesh coordinates [26]. Moreover, we will need the values of K_x and K_y at point $p11$ and $p12$. These values can be estimated using interpolation functions such as

$$(K_x)_{p11} = \sum_{j=1}^3 K_{x,j} \psi_j(x_{p11}, y_{p11}) \quad (21)$$

$$\text{and } (K_y)_{p11} = \sum_{j=1}^3 K_{y,j} \psi_j(x_{p11}, y_{p11})$$

where $K_{x,j}$ and $K_{y,j}$ are respectively the given values of K_x and K_y at node j .

At this stage of development, we have completely defined the coefficients of the first row of the elementary stiffness matrix \mathbf{K}_T . By adopting the notations of the Figure 2, the two other rows of the matrix \mathbf{K}_T are obtained in a similar way by

For Sub-Control Volume \mathcal{S}_2

$$\begin{aligned} \int_{[b,g]} (\overline{\overline{\mathbf{K}}} \nabla \varphi) \vec{n} dl + \int_{[g,a]} (\overline{\overline{\mathbf{K}}} \nabla \varphi) \vec{n} dl &= \sum_{j=1}^3 \varphi_j \\ &\cdot \left[(K_x \alpha_j^T n_{21}^x + K_y \beta_j^T n_{21}^y)_{p21} \ell_{21} \right. \\ &\quad \left. + (K_x \alpha_j^T n_{22}^x + K_y \beta_j^T n_{22}^y)_{p22} \ell_{22} \right] \end{aligned} \quad (22)$$

For Sub-Control Volume \mathcal{S}_3

$$\int_{[c,g]} (\overline{\overline{K}} \nabla \varphi) \vec{n} dl + \int_{[g,b]} (\overline{\overline{K}} \nabla \varphi) \vec{n} dl = \sum_{j=1}^3 \varphi_j \cdot \left[(K_x \alpha_j^T n_{31}^x + K_y \beta_j^T n_{31}^y)_{p31} \ell_{31} + (K_x \alpha_j^T n_{32}^x + K_y \beta_j^T n_{32}^y)_{p32} \ell_{32} \right] \quad (23)$$

Finally a generalization of the elementary stiffness matrix \mathbf{K}_T (3x3) gives

$$(K_T)_{ij} = \left[(K_x \alpha_j^T n_{i1}^x + K_y \beta_j^T n_{i1}^y)_{pi1} \ell_{i1} + (K_x \alpha_j^T n_{i2}^x + K_y \beta_j^T n_{i2}^y)_{pi2} \ell_{i2} \right] \quad (24)$$

$i = 1, 2, 3 \quad j = 1, 2, 3$

In the same way, the second elementary element vector \mathbf{b}_T has the following components: $(S_m \text{mes}(\mathcal{S}_m))_{m=1,2,3}$. Where S_m is the value of the source term at the node m . if we note by $\Psi_T = (\varphi_1, \varphi_2, \varphi_3)$ the elementary solution vector, we can write

$$\mathbf{M}_T \frac{\partial \Psi_T}{\partial t} + \mathbf{K}_T \Psi_T = \mathbf{b}_T \quad (25a)$$

$$\begin{bmatrix} \text{mes}(\mathcal{S}_1) & 0 & 0 \\ 0 & \text{mes}(\mathcal{S}_2) & 0 \\ 0 & 0 & \text{mes}(\mathcal{S}_3) \end{bmatrix} \frac{\partial \Psi_T}{\partial t} + \begin{bmatrix} (K_T)_{11} & (K_T)_{12} & (K_T)_{13} \\ (K_T)_{21} & (K_T)_{22} & (K_T)_{23} \\ (K_T)_{31} & (K_T)_{32} & (K_T)_{33} \end{bmatrix} \Psi_T = \begin{bmatrix} S_1 \text{mes}(\mathcal{S}_1) \\ S_2 \text{mes}(\mathcal{S}_2) \\ S_3 \text{mes}(\mathcal{S}_2) \end{bmatrix} \quad (25b)$$

To solve equation (13), global matrices \mathbf{M} , \mathbf{K} , \mathbf{b} can now be obtained by the classical FEM assembly procedure of the elementary matrix by

$$\begin{aligned} \mathbf{M} &= \sum_{T \in \mathcal{T}_h} \mathbf{M}_T \\ \mathbf{K} &= \sum_{T \in \mathcal{T}_h} \mathbf{K}_T \\ \mathbf{b} &= \sum_{T \in \mathcal{T}_h} \mathbf{b}_T \end{aligned} \quad (26)$$

The sum sign in the expression (26) designates the assembly operation. It should be noted that the code developed in this study solves Darcy's equation for stationary flow (i.e. $\partial \Psi / \partial t = 0$). In this case the discrete linear system (13) is reduced to

$$\mathbf{K} \Psi = \mathbf{b} \quad (27)$$

Finally, to solve the linear system resulting from the discretization procedure of the equation (3) (in steady state), we tested several iterative methods for sparse matrices (Gauss-Seidel, BiCG, BiCG-Stab, GMRES, ...) with pre-conditioner (diagonal, IC, ILU(k), MILU, ...) but also the direct method based on Gauss elimination for sparse matrices. From these tests, it was concluded that it is the BiCGStab method preconditioned by ILU(0) that provided the best results (convergence obtained about 20 iterations for 10^{-16} of tolerance).

2.5. Optimization Procedure (Genetic Algorithm). Several methods have been proposed to solve linear and nonlinear optimization problems. These methods have been classified into two categories: methods with gradients and methods without gradients (Goldberg, 1989). The methods with gradients of iterative type are efficient and less expensive in computing time when the objective function is fairly regular. However, this type of method also suffers from the inability to provide a global optimum. They also have the disadvantage of not being applicable to objective functions of discontinuous derivatives. The second category qualified to the random search was proposed because of the shortcomings of the first category. Thus, the optimization methods based on the random search do not use any computation of derivatives, but only based on a research step followed by objective function evaluation as many times as necessary for the convergence towards the global optimum. In this category the most popular methods are genetic algorithms and evolution strategy algorithms. We recall that in this study we adopted the genetic algorithm to solve the optimization step to identify the transmissivity field.

Genetic algorithms are inspired by the evolution of species in their natural environments. These methods consider that species adapt optimally to their living environments in perpetual evolution: the individuals of each species must reproduce to generate a new "better" individuals when some improvement criteria are imposed. In the rest of the paper, we will use a terminology borrowed from biologists and geneticists to represent each of the concepts used in this paper. Indeed, a population refers to a set of individuals. In the same way, an individual will be a solution to the studied problem. Moreover, a gene will designate a component of a solution, therefore, of an individual. Finally, a generation is an iteration of the algorithm seeking the global optimum of the problem.

As stated above, the GA operates on the Darwinian principle of survival of the most able individual of a population. GA starts with an initial population (generally chosen randomly) that will evolve in order to improve its individuals. Therefore, during the generation some individuals undergo modifications while others disappear to give place to the new, more efficient individuals (more fit). One understands then that the GA operates on a population and is not on a particular individual. Thus an GA takes place in five phases that we explain below:

- (i) The generation of the initial population;
- (ii) The evaluation of individuals;
- (iii) The creation of a new individual;

- (iv) The insertion of new individuals into the population;
- (v) Reiterations of the generation.

The GA begins by generating in the search space an initial population created randomly. Randomness is adopted in order to diversify individuals to increase the chances of generating the best possible solutions. The size of the population N is not restricted, but a size of 100 or 150 individuals is usually a good compromise between the quality of the solutions and the execution time of the algorithm.

Once the population is created, the evaluation of its individuals is made to decide the performance of those who will be selected for the improvement of the population. So, the evaluation stage consists of assigning a quality score of individuals. There are several methods of evaluation, for example, methods using the notion of dominance: in fact, one individual dominates another if it is better in each of the criteria on which the evaluation is based. An evaluation method consists of measuring the rank of an individual who is defined as the number of individuals who dominate it +1. In the sense of this measure it is well understood that the best individuals are those of the lowest rank. It should be noted that the evaluation stage of the individuals can be carried out before and/or after the crossover and mutation steps.

In order to diversify and enrich a new population, we must create new individuals while keeping the efficient individuals. This operation is performed by crossing individuals selected by their rank to be able to participate in the generation of new individuals. Thus the generated individual results from the crossover operation of the few genes of the two individuals in the current population. For example, individual 1 has the genetic sequence (ABCDEF), individual 2 has the genetic sequence (0123456), and a possible new individual will carry the genes (ABCD456). This is what is called a single crossover (only one crossing point, here is the point between D and 4). Note that it is possible to consider a multiple points crossover operation.

Despite all these improvements, it is possible that the joint action of the selection and crossover operations does not allow to converge to the optimal solution of the problem. Indeed, assume a population with individuals of single chromosome. Consider a particular gene of this chromosome, called G. This gene has 2 possible alleles: 0 and 1; if no individual in the initial population possesses allele 1 for this gene, no possible crossover operation can introduce this allele for the gene G. Consequently, if the optimal solution of the problem is such that the gene G must have allele 1, it will be impossible to reach this optimal solution only by selection and crossover operations. In geneticist language, this situation is known as genetic degeneration. To avoid such situation during the implementation of GA, we must introduce a new operation called "mutation". This operation consists in changing the allelic value of a gene according to a very low probability p_m ($0.001 < p_m < 0.01$). In other words, the mutation operator reverses randomly one bit (or several, but given the low probability to this operation, it is extremely rare) of the chromosome sequence of an individual. It is then understood that the mutation randomly changes the characteristics of a solution. Like crossover

operation, the mutation operation allows to introduce and maintain diversity in the solutions population. We can also interpret the mutation as a "noise" randomly introduced into the population.

Finally, note that the mutation is a very important operation for the convergence of an GA towards the global optimum. Indeed, this operation is analogous to the mathematical property of ergodicity which guarantees that any element of the search space can be explored. By analogy, the mutation acts randomly on any bit of the chromosome. As a result, any inversion of the bit string can appear in the current population and therefore any solution in the search space can be reached. This observation then shows that mutation ensures convergence towards the optimal solution of the studied problem.

At this stage, new individuals have been generated jointly by crossing operations and mutations. Now, it remains to select among the newly created individuals those who will participate in the improvement of the current population. In addition, selection must be based on a measure of the performance of new individuals. For example, performance can be evaluated by calculating the rank of individuals defined above. It should be noted that the size N of the population also remains to be determined. Indeed, the choice of the size N too low risks becoming progressively weaker as we advance in the generation until the disappearance of the population. Similarly, if size N is large, it may increase significantly the time execution of the algorithm. It is therefore recommended to keep the same population size from one generation to the next.

Once the new population is obtained, the process of improving the individuals will be repeated to generate the new population, and so on. The process will be stopped as soon as we no longer observe a substantial evolution of individuals in the current population (this corresponds to a maximum number of generations). At the end of the program, we obtain a population of solutions from which we can extract the most efficient solution (measured by its rank). It is this solution that approaches the global optimum of the studied problem. Figure 3 illustrates the principle of building an GA generation.

3. Application of HySubF-CVFEM/GA Integrated Optimization Algorithm

Before applying the combination HySubF-CVFEM/GA to identify the real transmissivity field, we first validate this combination on a schematic case offering an analytical solution. This is to solve the following problem:

$$(\text{IP}) \begin{cases} \text{Minimize } F(\overline{\overline{K}}) \\ \overline{\overline{K}} \in \Omega_A \\ \text{under constraints} \\ (\text{DP}) \begin{cases} -\nabla \cdot (\overline{\overline{K}} \nabla \varphi) = S & \text{in } \Omega \\ \varphi = \varphi_D & \text{in } \partial\Omega_D \\ \vec{n} \cdot \vec{q} = \varphi_N & \text{in } \partial\Omega_N \end{cases} \end{cases} \quad (28)$$

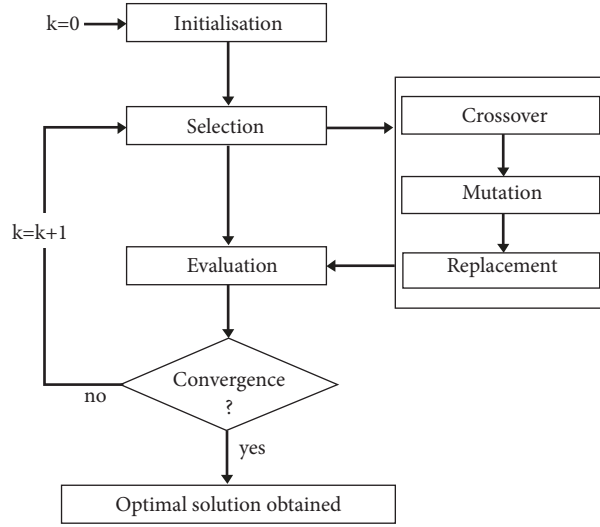


FIGURE 3: The schematic diagram of one generation in GA.

where Ω_A is the admissible set values of the tensor and F is the objective function given by

$$F(\bar{K}) = \|\varphi_{obs} - \varphi(\bar{K})\| \quad (29)$$

Figure 4 illustrates the computations sequence of the proposed integrated optimization algorithm. The convergence of this algorithm will provide the optimal solution \bar{K}_{opt} which is none other than the desired transmissivity fields.

$$\bar{K}_{opt} = \min_{\bar{K} \in \Omega_A} \|\varphi_{obs} - \varphi(\bar{K})\| \quad (30)$$

In addition to the stability problems that the HySubF-CVFEM/GA coupling can generate by the use of the poor accurate solution, it should be noted that the inverse problems can be confronted to the uniqueness solution problem. Indeed, different hydrological configurations can provide identical observations φ_{obs} . Therefore, it is difficult (if not impossible) to uniquely identify a particular aquifer situation solely from the observations. In Smaoui et al. 2018, the reader will find some methods adopted to ensure the uniqueness of the solution of the inverse problem in hydrogeology.

3.1. Numerical Test (Validation Case). To verify the performance of the proposed coupling to identify by optimization the transmissivity fields, we apply this methodology to an inverse problem with an analytical solution. This exercise allows us to validate the HySubF-CVFEM/GA coupling, but also to estimate the error level by evaluating the difference between the analytical and numerical solutions obtained by the developed, integrated optimization model HySubF-CVFEM/GA. It should be noted that we have made comparisons with the results of other authors [27] solving the inverse problem for real cases by other optimization methods based on gradient methods. These comparisons were made to verify the ability of HySubF-CVFEM/GA

to reproduce the real case solution performed by these authors. It emerges from these comparisons that the HySubF-CVFEM/GA coupling has allowed to obtain the global optimal solution with excellent accuracy, but with a convergence speed approaching unity (significant computation time). It should be noted that this validation test was studied by Smaoui et al. [19], but for another integrated optimization algorithm called HySubF-FEM/CMA-ES which differs from the present model both by method solving the direct problem (finite element method) and by the optimization method (CMA-ES: Covariance Matrix Adaptation Evolution Strategy) that is based on evolution algorithms. The details of these comparisons are presented in Smaoui et al. [19].

In this paper, we present the results of an inverse problem with an analytical solution. This is the solution of the 2D direct problem on a rectangular domain $\Omega = [0, a] \times [0, b]$ with a given isotropic transmissivity linear field in the form $\bar{K}(x, y) = \alpha(x + y)$ and Dirichlet boundary condition type. The problem to be solved can be formulated by

$$(DP) \begin{cases} -\nabla \cdot (\bar{K} \nabla \varphi) = S & (x, y) \in \Omega \\ \varphi = \varphi_D & (x, y) \in \partial\Omega \end{cases} \quad (31)$$

with form $S(x, y) = -6\alpha\beta(x + y)$ and $\varphi_D(x, y) = \varphi_{exact}(x, y)$ on the domain boundary $\partial\Omega$. The exact solution of the problem (31) reads

$$\varphi_{exact}(x, y) = \beta(x^2 + y^2) \quad (32)$$

It should be remembered that the aim of this exercise is to solve the inverse problem. That is to say, given the solution φ_{exact} is the proposed HySubF-CVFEM/GA able to find the optimal solution? which in this case is exactly the function

$$\bar{K}(x, y) = \begin{bmatrix} T(x, y) & 0 \\ 0 & T(x, y) \end{bmatrix} \quad (33)$$

with $T(x, y) = \alpha(x + y)$.

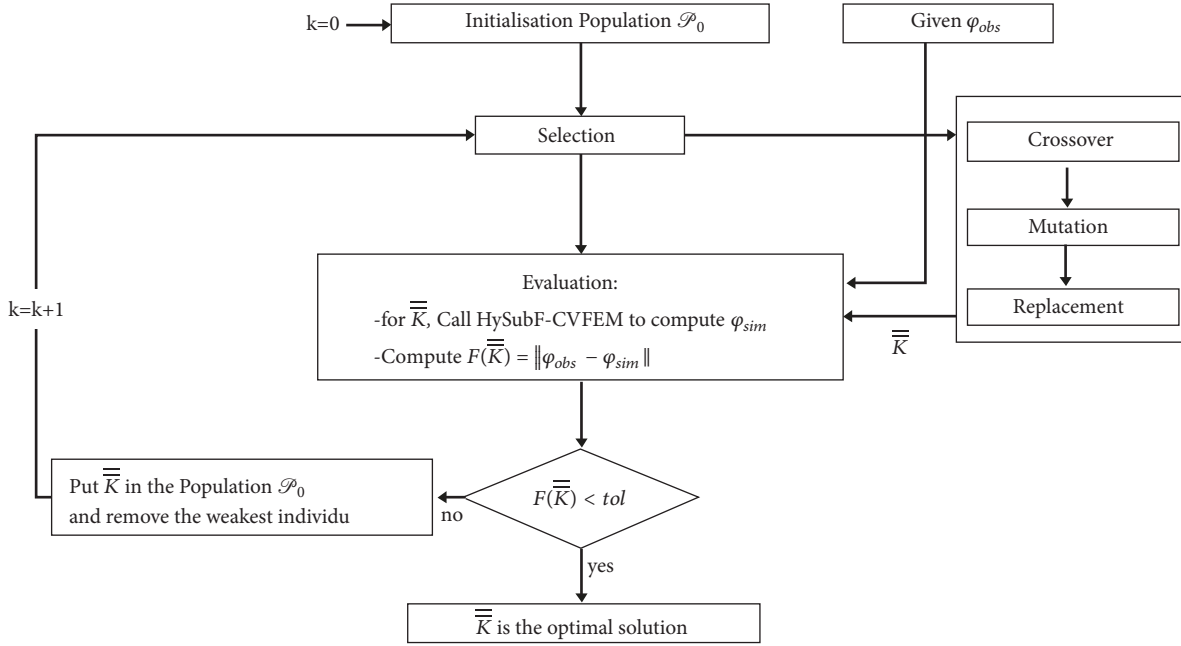


FIGURE 4: The integrated optimization algorithm (coupling of the *HySubF-CVFEM/GA* model).

This problem has already been studied by Smaoui et al., [19] with $a = 3500m$; $b = 2000m$; $\alpha = 10^{-5}$; $\beta = 10^{-6}$. With the a and b values, the function T is bounded between 0 and $\alpha(a + b)$. These two limit values were useful to use the version of integrated optimization model HySubF-CVFEM/GA with constraints to limit the research space to the admissible values and thus saving time of computation.

It is the algorithm illustrated in Figure 4 that has been applied to this test case. Analysis of simulation results showed that the model has identified the field T with excellent accuracy. The L_∞ absolute error is about $3.5 \times 10^{-5} m^2 s^{-1}$, while the relative error ($\|T_{exact} - T_{identified}\| / \|T_{identified}\|$) does not exceed 1%. We also study the behavior of the convergence of the proposed algorithm. Indeed, the evolution curve of the objective function as a function of iteration numbers (not shown here) shows that during the first 2500 generations the value of the objective function is 10^{-3} to reach the value 2.1×10^{-4} for 3200 generations. This observation allows us to conclude that genetic algorithms are relatively fast at the beginning of the research process, but stagnate when we approach convergence. This finding is not surprising and is inherent in the design of the GAs. Indeed, at the beginning of the search stage the AG needs to look for an improvement among a vast population. It is therefore easy to find better solutions of the previous ones. However, as the process progresses, there is a population with only the best solutions. As a result, it becomes difficult to improve the solutions. This translates into a minimal gain in accuracy at the end of the search process. In other words, near convergence, AGs continue to make generations to gain only a few significant digits in precision. The slowness of GA near convergence has already been observed by the several authors using genetic algorithms as optimization tools [28].

Figure 6 summarizes the comparison between the analytical solution T_{exact} and the numerical solution $T_{identified}$. It presents the identified transmissivity according to the exact transmissivity. On this graph a 1:1 straight slope curve has been superimposed to assess the absolute difference between the exact solution and the solution identified by our code HySubF-CVFEM/GA. One can see a good agreement between the two solutions. This figure illustrates also that the relative error does not exceed 1% as mentioned above. In our opinion the high accuracy of the results obtained for this schematic case is due to the nature of the PDE equation which governs the direct problem (second-order elliptic), but also the schematic case treated by HySubF-CVFEM/GA is an well-posed constrained optimization problem.

3.2. Realistic Case. The coastal aquifers play an important role in the in the socioeconomic development of the coastal plains. These costal aquifers are particularly exposed to overexploitation problems that can induce aquifer salinization. Also, as presented in the Intergovernmental Panel on climate change (IPCC, 2007), climate changes that will provide variations in the sea level, temperature and rate and intensity of precipitation. All these changes will affect freshwater resources, both in terms of quantity and quality [8].

For several decades, observations by hydrogeologists in the Chaouia region (Figure 7) have led to significant drops in the water table, but also with the risk of saline invasion. It is therefore urgent to have a numerical tool capable of simulating the behavior of this aquifer system. It is in this context that we apply the integrated optimization model HySubF-CVFEM/GA to the Chaouia coastal plain located along the Atlantic coast of Morocco. It extends from Casablanca to

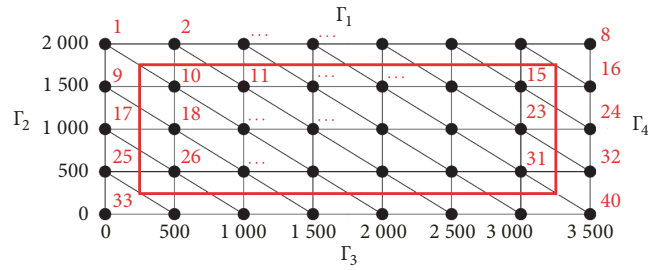


FIGURE 5: Mesh of the studied domain and internal nodes [19].

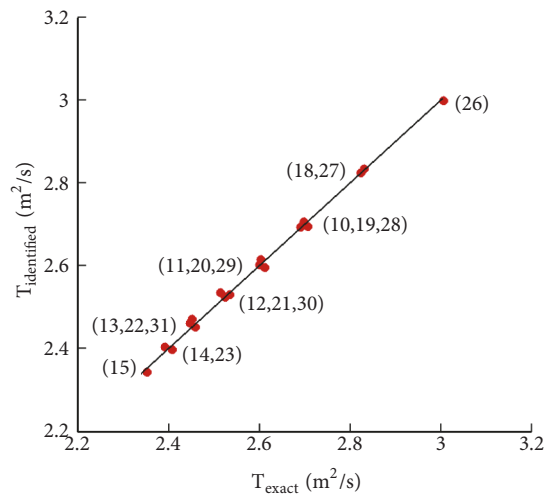


FIGURE 6: Exact versus identified transmissivity with a line of 1:1 slope. Values in parentheses indicate the node number of the mesh plotted in Figure 5 [19].

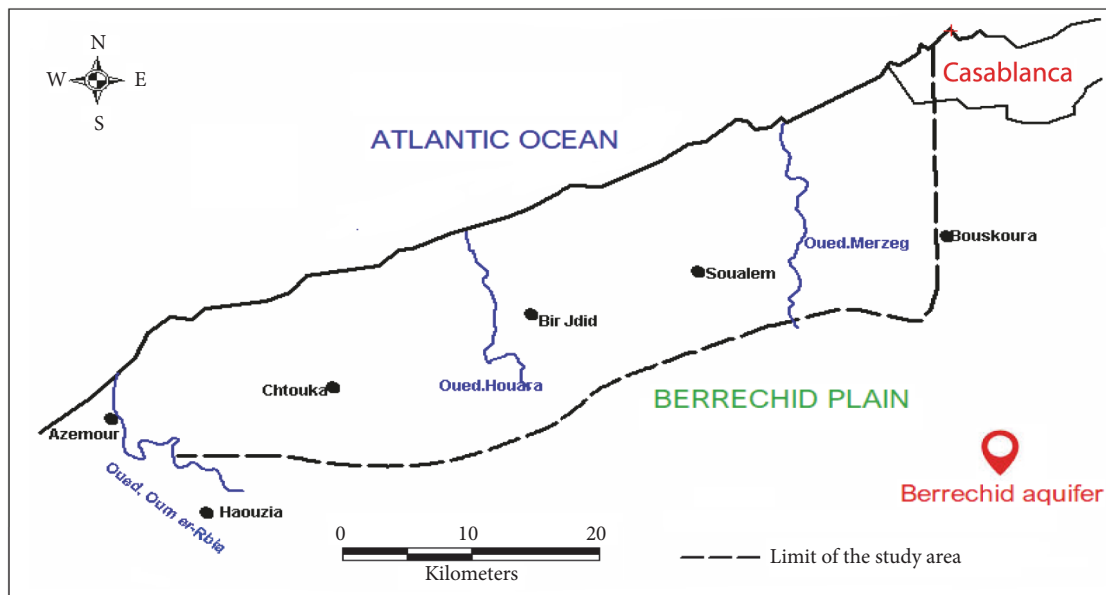


FIGURE 7: Location of the Chaouia coastal aquifer [20].

Azemmour over a distance of 65 km and a width of 15 to 20 km corresponding to a surface of about 1100 km² [29]. This area represents a fairly flat surface with only a few sandy dunes parallel to the Atlantic Ocean (See Figure 7 for location). The Chaouia coastal aquifer constitutes an important aquifer in west Morocco where the irrigated agriculture farming is the main economic resource of the region. This aquifer is subject to intensive water pumping and water quality deterioration by salinization. For these reasons, the hydrogeological modeling became an important way to evaluate water resource and quality for aquifers management. The HySuf-CVFEM/GA code is used to identify the transmissivity field of the Chaouia coastal aquifer.

Based on the geological formation, groundwater in the Chaouia aquifer exists from place to place in the Paleozoic schist, in the Cretaceous or in the Plio-Quaternary formation and for each aquifer, the thickness is included between 5 and 20 m (Mostadraf et al., 2008). It is important to recall that there are vertical and horizontal hydraulic communications between these aquifers. Different pumping tests were performed in the studied area with the objective to evaluate the aquifer transmissivity. The obtained values are included between $10^{-5} \text{ m}^2 \text{ s}^{-1}$ and $3.62 \times 10^{-2} \text{ m}^2 \text{ s}^{-1}$ and the mean value corresponds to $2.62 \times 10^{-2} \text{ m}^2 \text{ s}^{-1}$. Otherwise piezometric maps of the Chaouia coastal aquifer were performed by different authors showing that the water flow is uniformly directed towards the Atlantic Ocean except in the southern part of the groundwater where the water flows from the East to the West.

It should be noted that the numerical model HySuf-CVFEM was validated for hydrodynamics by comparison with analytical solution, then by comparison with the results of other numerical model massively used in modeling of the underground flows. The analysis of the results of the comparisons showed that the model HySuf-CVFEM reproduces with a good precision the flow studied. From these comparisons, it was also concluded that our numerical model provides good mass conservation which is a fundamental property in fluid flow. The results of these comparisons are not presented in this paper, but can be found in Smaoui et al., [26]

The chosen area for HySuf-CVFEM/GA model application is extended to an area about 800 km². It is limited by the Atlantic Ocean at the North-West, the Oum-Erbia river at the South-West, the El Hank at the North-East and the Berrechid plain to the South-East (Figure 7). Taking into account the real geometry of the aquifer and its hydrogeological characteristics, we have constructed a numerical model of the Chaouia aquifer discretized in triangular mesh of 5100 nodes and 9922 elements. For boundary conditions, we have adopted the following conditions. We impose the condition of zero flux (Neumann condition) along El Hank at north-east and at along the streamline connecting the upstream limit to the Oum-Erbia river. On the Atlantic coastline we have imposed a head (Dirichlet condition) corresponding to the sea level which constitutes a natural outflow of the water table. Finally, at the Berrechid plain and Oum-Erbia river mixed boundary condition was imposed depending on a given load. To complete the data necessary for the calculation process,

we have estimated the recharge that is done by infiltration of rainwater. This recharge corresponds to 15% of the rainfall. The effective rainfall was thus calculated using daily precipitation to obtain $1.62 \times 10^{-9} \text{ m s}^{-1}$ per triangular element. To complete the data necessary for the calculation, infiltration values were estimated from the daily water balance, which were computed using the Thornthwaite method. The effective rainfall was thus calculated using daily precipitation to obtain $12.6 \times 10^{-3} \text{ m}^3 \text{ s}^{-1}$ per triangular element.

3.3. Results Interpretation and Discussion. Calculated (red) and measured (blue) piezometric level are presented in Figure 8. This last figure shows a perfect agreement between the two piezometric levels. The difference between these two values does not exceed 2 m at the 160 m and the relative error is about 1.0%. Considering the measurement errors of the piezometric levels that are related to the wells elevations and to water depths, these differences can be considered as acceptable.

The calculated transmissivity using the proposed code is shown in Figure 9. This figure indicates that the obtained transmissivity has a heterogeneous distribution over the studied area. These calculated values of this hydrogeological parameter are included between 10^{-5} and $10^{-2} \text{ m}^2/\text{s}$.

Based on this transmissivity distribution, two distinguished areas can be identified:

- (i) the first one, with high transmissivity that can reach the values higher than $10^{-2} \text{ m}^2/\text{s}$; these are located: (i) around and in the north coastal area of the Bir jdid city and (ii) around Oum Rbia river;
- (ii) the second areas with lower transmissivity values (lower than $2.10^{-3} \text{ m}^2/\text{s}$) are located in the intermediate zone between coastal area and south part of the studied area.

Different factors can explain the transmissivity distribution in the studied area:

- (i) The aquifer lithology: the higher transmissivity values are related to Pliocene and Quaternary formations; however, the lower transmissivity is related to presence of Cenomanian marly-limestone formation in the southwest of the studied area and to Palaeozoic bedrock formation in the east part of studied area;
- (ii) The aquifers thickness which are included between 5 and 20 m [30].

Finally, it is important to recall that the calculated values are in the same range than those obtained using pumped test.

4. Conclusions

Most of the hydrogeological parameter identification problems have been formulated and solved by gradient optimization methods. These methods may prove unusable when the objective function is not regular enough. In addition, when convergence towards the optimum is ensured, this type of method generally converges towards a local optimum.

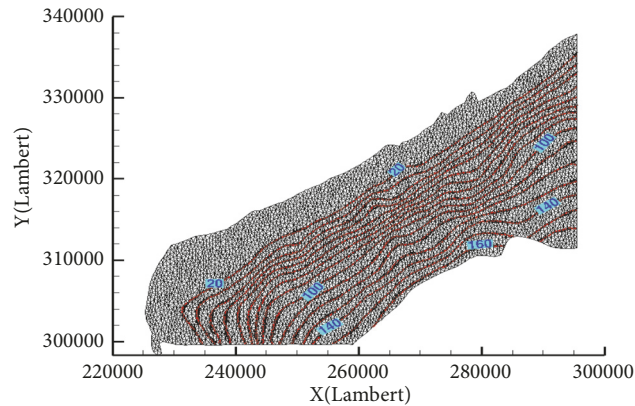


FIGURE 8: Head comparison: measured and computed from the HySuF-CVFEM/GA model. (red line= measures, black line= computation).

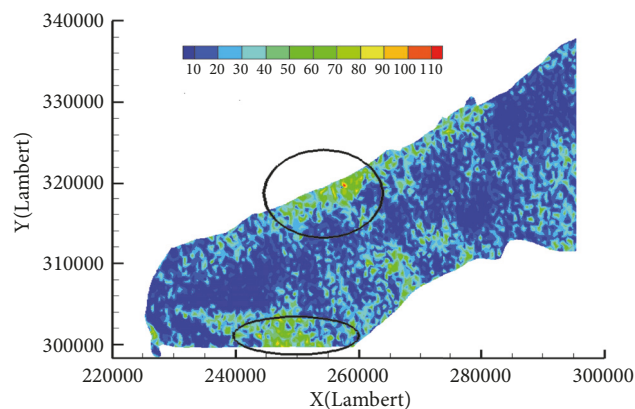


FIGURE 9: Identified transmissivity field of Chaouia aquifer by HySuF-CVFEM/GA model. (values must be multiplied by 10^{-7} factor).

In recent years we have been witnessing the emergence of metaheuristic optimization methods and, more specifically, genetic algorithms (GA). On one hand, this type of method does not require a minimum of regularity of the objective function; on the other hand, these methods converge towards a global minimum. This paper deals with solving the inverse problem by coupling two computation codes: the first is the HySuF-CVFEM code to solve the direct problem and the second is the code of the genetic algorithm to solve the optimization problem. Our choice was for the GA for the optimization phase is for not only to focus on demonstrating the regularity of the objective function, but also to ensure convergence towards a global optimum. The proposed HySuF-CVFEM/GA integrated optimization algorithm has been validated by comparison with analytical solutions. This comparison showed that the code thus constructed HySuF-CVFEM/GA is able to provide (by identification) a real transmissivity field of excellent quality. This coupling method has also been applied to the real case of the coastal aquifer of the “Chaouia” region in Western Morocco and has identified complex domains characterizing the heterogeneity of this aquifer. Nevertheless, it should be noted that the major disadvantage of HySuF-CVFEM/GA coupling remains the longer time required to reach convergence towards the global optimum. To avoid this inconvenience, we plan to use

parallel computing techniques for HySuF-CVFEM/GA coupling. Similarly, we will consider GA coupling with Kriging methods that are beginning to emerge in the identification parameters in hydrogeological research. Another interesting way is to attempt model reduction techniques to reduce the number of components of the variable vector. These techniques will be based on orthogonal decomposition (POD) and properly generalized decomposition (PGD) methods.

Data Availability

The data used to support the findings of this study are available from the corresponding author upon request.

Conflicts of Interest

The authors declare that they have no conflicts of interest.

Acknowledgments

The authors wish to thank the anonymous reviewers for their constructive criticism that led to the improvement of the manuscript.

References

- [1] J. F. Carneiro, M. Boughriba, A. Correia, Y. Zarhloule, A. Rimi, and B. El Houadi, "Evaluation of climate change effects in a coastal aquifer in Morocco using a density-dependent numerical model," *Environmental Earth Sciences*, vol. 61, no. 2, pp. 241–252, 2010.
- [2] Y. Fakir, A. Zerouali, M. Aboufirassi, and M. Bouabdelli, "Exploitation et salinité des aquifères de la Chaouia côtière, littoral atlantique," *Journal of African Earth Sciences*, vol. 32, no. 4, pp. 791–801, 2001.
- [3] Y. Fakir and M. Razack, "Hydrodynamic characterization of a Sahelian coastal aquifer using the ocean tide effect (Dridrate Aquifer, Morocco)," *Hydrological Sciences Journal*, vol. 48, no. 3, pp. 441–454, 2003.
- [4] B. Benseddik, E. El Mrabet, B. El Mansouri, J. Chao, and M. Kili, "Delineation of artificial recharge zones in Mnasra Aquifer (NW, Morocco)," *Modeling Earth Systems and Environment*, vol. 4, pp. 3–10, 2017.
- [5] A. D. Koussis, K. Mazi, and G. Destouni, "Analytical single-potential, sharp-interface solutions for regional seawater intrusion in sloping unconfined coastal aquifers, with pumping and recharge," *Journal of Hydrology*, vol. 416–417, pp. 1–11, 2012.
- [6] A. D. Koussis and K. Mazi, "Corrected interface flow model for seawater intrusion in confined aquifers: relations to the dimensionless parameters of variable-density flow," *Hydrogeology Journal*, vol. 26, no. 8, pp. 2547–2559, 2018.
- [7] P. M. Carreira, M. Bahir, O. Salah, P. Galego Fernandes, and D. Nunes, "Correction: Tracing salinization processes in coastal aquifers using an isotopic and geochemical approach: comparative studies in western Morocco and southwest Portugal," *Hydrogeology Journal*, vol. 26, no. 8, p. 2933, 2018.
- [8] B. C. Bates, Z. W. Kundzewicz, S. Wu, and J. P. Palutikof, *Technical Paper on Climate Change and Water*, IPCC, Cambridge University Press, Cambridge, UK, 2008.
- [9] P. O. Yapo, H. V. Gupta, and S. Sorooshian, "Multi-objective global optimization method for hydrological models," *Journal of Hydrology*, vol. 204, pp. 204–83, 1998.
- [10] J. Morshed and J. J. Kaluarachchi, "Application of artificial neural network and genetic algorithm in flow and transport simulations," *Advances in Water Resources*, vol. 22, no. 2, pp. 145–158, 1998.
- [11] D. K. Karpouzou, F. Delay, K. L. Katsifarakis, and G. De Marsily, "A multipopulation genetic algorithm to solve the inverse problem in hydrogeology," *Water Resources Research*, vol. 37, no. 9, pp. 2291–2302, 2001.
- [12] Q. Duan, J. Schaake, V. Andréassian et al., "Model Parameter Estimation Experiment (MOPEX): an overview of science strategy and major results from the second and third workshops," *Journal of Hydrology*, vol. 320, no. 1–2, pp. 3–17, 2006.
- [13] K. C. Abbaspour, C. A. Johnson, and M. T. van Genuchten, "Estimating uncertain flow and transport parameters using a sequential uncertainty fitting procedure," *Vadose Zone Journal*, vol. 3, no. 4, pp. 1340–1352, 2004.
- [14] M. H. Tber, M. El Alaoui Talibi, and D. Ouazar, "Parameters identification in a seawater intrusion model using adjoint sensitive method," *Mathematics and Computers in Simulation*, vol. 77, no. 2–3, pp. 301–312, 2007.
- [15] K. A. Tapes and A. K. Rastogi, "Artificial neural network application on estimation of aquifer transmissivity," *Journal of Spatial Hydrology*, vol. 8, no. 2, pp. 15–31, 2008.
- [16] H. Hashemi, R. Berndtsson, M. Kompani-Zare, and M. Persson, "Natural vs. artificial groundwater recharge, quantification through inverse modeling," *Hydrology and Earth System Sciences*, vol. 17, no. 2, pp. 637–650, 2013.
- [17] W. W.-G. Yeh, "Review of parameter identification procedures in groundwater hydrology: the inverse problem," *Water Resources Research*, vol. 22, no. 2, pp. 95–108, 1986.
- [18] J. Carrera, "State of the art of the inverse problem applied to the flow and solute transport equations," in *Groundwater Flow and Quality Modelling*, E. Custodio, A. Gurgui, and J. P. Ferreira, Eds., vol. 224 of *NATO ASI Series (Series C: Mathematical and Physical Sciences)*, pp. 549–583, Springer, Dordrecht, Netherlands, 1988.
- [19] H. Smaoui, L. Zouhri, S. Kaidi, and E. Carlier, "Combination of FEM and CMA-ES algorithm for transmissivity identification in aquifer systems," *Hydrological Processes*, vol. 32, no. 2, pp. 264–277, 2018.
- [20] J. Moustadraf, *Modélisation numérique d'un système aquifère côtier : Etude de l'impact de la sécheresse et de l'intrusion marine. La Chaouia Côtière, Maroc*, Thèse de Doctorat de l'Université de Poitiers, France, 2006.
- [21] P. G. Ciarlet, "The finite element method for elliptic problems," in *Classics in Applied Mathematics*, p. 530, SIAM, Philadelphia, Pa, USA, 1978.
- [22] R. Huber and R. Helmig, "Node-centered finite volume discretizations for the numerical simulation of multiphase flow in heterogeneous porous media," *Computational Geosciences*, vol. 4, no. 2, pp. 141–164, 2000.
- [23] G. Manzini and S. Ferraris, "Mass-conservative finite volume methods on 2-D unstructured grids for the Richards' equation," *Advances in Water Resources*, vol. 27, no. 12, pp. 1199–1215, 2004.
- [24] B. R. Baliga and S. V. Patankar, "A new finite-element formulation for convection-diffusion problems," *Numerical Heat Transfer*, vol. 3, no. 4, pp. 393–409, 1980.
- [25] B. R. Baliga and S. V. Patankar, "A control volume finite-element method for two-dimensional fluid flow and heat transfer," *Numerical Heat Transfer*, vol. 6, no. 3, pp. 245–261, 1983.
- [26] H. Smaoui, L. Zouhri, and S. Kaidi, "Parameters identification in hydrogeology by using the CMA-ES algorithm," Research Report No 2015.1, Cerema /DTecEMF, Compiègne, France, 2015.
- [27] F. T.-C. Tsai, N.-Z. Sun, and W. W.-G. Yeh, "A combinatorial optimization scheme for parameter structure identification in ground water modeling," *Groundwater*, vol. 41, no. 2, pp. 156–169, 2003.
- [28] S. Baluja, "Structure and performance of fine Frain parallelism in genetic search," in *Practical Handbook of Genetic Algorithms*, L. Chmabers, Ed., vol. 2, pp. 139–154, New Frontiers, Boca Raton, Fla, USA, 1995.
- [29] A. Marjoua, P. Olive, and C. Jusserand, "Apports des outils chimiques et isotopiques à l'identification des origines de la salinisation des eaux : Cas de la nappe de La Chaouia côtière (Maroc)," *Journal of Water Science*, vol. 10, no. 4, pp. 489–505, 1997.
- [30] A. Marjoua, *Approche géochimique et modélisation hydrodynamique de l'aquifère de la Chaouia Côtière (Maroc) : Origines de la salinisation des eaux*, Thèse de doctorat de l'université Paris VI, France, 1995.



Hindawi

Submit your manuscripts at
www.hindawi.com

